DMD Fast Forward. Published on January 12, 2018 as DOI: 10.1124/dmd.117.078808
This article has not been copyedited and formatted. The final version may differ from this version.

A study on pharmacokinetics of bosentan with systems modeling, Part 2: prospectively predicting systemic and liver exposure in healthy subjects

Rui Li, Emi Kimoto, Mark Niosi, David A. Tess, Jian Lin, Larry M. Tremaine, Li Di

Systems Modeling and Simulation, Medicine Design, Pfizer Worldwide R&D, Cambridge, MA (RL); Pharmacokinetics, Dynamics and Metabolism, Medicine Design, Pfizer Worldwide R&D, Groton, CT (EK, MN, DAT, JL, LMT, and LD).

Running title

Predicting human systemic and liver exposure of bosentan

Corresponding Author

Rui Li. Systems Modeling and Simulation, Medicine Design, Pfizer Worldwide R&D, Cambridge, MA. Phone: 617-551-3340. Email: Rui.Li5@pfizer.com

Number of text pages: 15

Number of tables: 4

Number of Figures: 5

Number of references: 14

Number of words in Abstract: 160

Number of words in Introduction: 591

Number of words in Discussion: 1250

DMD Fast Forward. Published on January 12, 2018 as DOI: 10.1124/dmd.117.078808
This article has not been copyedited and formatted. The final version may differ from this version.

Abbreviations

CYP: cytochrome P450

DDI: drug-drug interaction

ET: endothelin receptors,

IVIVE: *in vitro* to *in vivo* extrapolation

Kp_{uu}: unbound tissue-to-unbound systemic plasma concentration ratio

Kp_u: total tissue-to-unbound systemic plasma concentration ratio

MCMC: Markov chain Monte Carlo

OATP: organic anion transporting polypeptide

PBPK: physiologically based pharmacokinetic

PD: pharmacodynamics

PET: positron emission tomography

PK: pharmacokinetics

PMH: plated monkey hepatocyte

RBC: red blood cells

SCHH: sandwich cultured human hepatocyte

RSV: rifamycin SV

DMD Fast Forward. Published on January 12, 2018 as DOI: 10.1124/dmd.117.078808
This article has not been copyedited and formatted. The final version may differ from this version.

Abstract

Predicting human pharmacokinetics of novel compounds is a critical step in drug discovery and clinical study design, but continues to be a challenging task for hepatic transporter substrates, particularly in predicting their liver exposures. In this study, using bosentan as an example, we have prospectively predicted systemic exposure and (pseudo) steady state unbound liver-to-unbound plasma ratio (Kp_{uu}) in healthy subjects using (1) a mechanistic approach solely based on *in vitro* hepatocyte assays, and (2) an approach based on hepatic process rates from monkey *in vivo* data but Michaelis–Menten constants from *in vitro* data. Both methods reasonably match the observed human systemic time course data, but the second method leads to a better prediction accuracy. In addition, the second method can predict a human Kp_{uu} that is almost identical to the value deduced using clinical data. We also generated rat and monkey liver Kp_{uu} in terminal studies. However, these directly measured animal values are different from the deduced human value.

Introduction

Predicting human pharmacokinetic (PK) profiles of novel drug candidates is critical in drug discovery and development to project dose, determine therapeutic index, and estimate drug-drug interaction (DDI) potential. With improved understanding on hepatic cytochrome P450 (CYP) activity, the relatively confident approaches have been developed in predicting hepatic CYP-mediated small molecule clearance. These approaches have enabled the chemistry design to reduce CYP-mediated metabolism for a prolonged drug half-life. However, such efforts have also led to an increased prevalence of hepatic-transporter-mediated clearance, for which understanding is still limited as of today. As a result, for hepatic transporter substrates, even with reasonable estimates of hepatic CYP activity and volume of distribution, the systemic exposure may be mis-predicted due to a failure in predicting liver exposure elevated or lowered by transporters. In addition, the ability to accurately predict liver exposure is also a foundation for predicting pharmacodynamics (PD), DDI, and drug-induced toxicity within the liver.

Most approaches developed to predict exposures of transporter substrates are based on *in vitro* assays. Unfortunately, most *in vitro* transport rates cannot describe *in vivo* data without empirical scaling factors (i.e. fudge factors closing the gap between physiological prediction and clinical observation), whether with a physiologically based pharmacokinetic (PBPK) model, or static pharmacokinetic equations (Li et al., 2014a). The empirical scaling factors are the primary limitations associated with approaches based on *in vitro* assays, because most published values are compound dependent and not readily available for novel compounds. Towards a prospective *in vitro* to *in vivo* extrapolation (IVIVE), Li et al. has developed an approach simultaneously leveraging data from multiple training compounds in empirical scaling factor estimation (e.g., global scaling factors that are not compound independent), assuming that substrates of the same or similar transporters share the same scaling factor (Li et al., 2014b). Animal studies are still an option for transporter substrates' PK predictions, particularly in understanding liver exposure, as global scaling factor estimations were based on systemic PK rather than liver concentration (Morse et al., 2015). However, the use of traditional inter-species scaling over-simplifies the physiological differences among species, and direct measurement in terminal or biopsy studies to understand tissue concentrations can be ambiguous and potentially misleading due to improper data interpretation or species differences in tissue exposure.

Most, if not all, of the methods published so far are only validated by systemic exposure, mainly because of the challenges in acquiring human liver data. Positron emission tomography (PET) has been proposed as a way to monitor liver drug concentration (Shimizu et al., 2012). However, PET studies are problematic due to being both expensive and to the fact that not all compounds can be easily prepared as PET ligands. Furthermore, PET signal can be confounded by metabolites formed in the liver (Li et al., 2014c). For the few compounds with minimal hepatic metabolism, transporter activity either has minimal impact on liver exposure (e.g., metformin) or there are additional challenges in studying PK (e.g., enterohepatic recirculation for pravastatin). Hence, using human liver exposure data to easily validate prediction methods remains atypical.

In this study, bosentan, an organic anion-transporting polypeptide (OATP) substrate was chosen as a prototype compound to (1) understand its liver exposure through analysis on systemic exposure, and (2) develop an approach to prospectively predict its liver exposure. In the Part 1 published in a separate article, human liver exposure of bosentan has been estimated from its systemic exposure using a "deduction" method. With the deduced bosentan liver exposure, we can compare the accuracy of both established and novel approaches to predict systemic and liver exposure in Part 2.

DMD Fast Forward. Published on January 12, 2018 as DOI: 10.1124/dmd.117.078808

Materials and Methods

Human and monkey hepatocyte uptake assay, and a mechanistic in vitro model

To understand the nonlinear transporter activity and intracellular binding processes, both sandwich cultured human hepatocyte (SCHH) and plated monkey hepatocyte (PMH) assays are performed with multiple dosing concentrations. The SCHH assay (lot HH1026, female donor, In Vitro ADMET, Columbia, MD) was carried out as described previously (Li et al., 2014c), except that 1 mM rifamycin SV (RSV) was used as transporter inhibitor. The method for PMH assay (lot 10106012, In Vitro ADMET, Columbia, MD) is provided in the supplemental materials.

A mechanistic model was developed to analyze the data. The model includes concentrations of unbound extracellular ($C_{HEP,UEC}$), unbound intracellular ($C_{HEP,UIC}$), bound intracellular compound ($C_{HEP,BIC}$), and intracellular binding sites available for non-specific binding ($C_{HEP,AST}$).

$$\begin{aligned} & V_{HEP,EC} \cdot \frac{dC_{HEP,UEC}}{dt} \\ & = CL_{HEP,pass} \cdot \left(C_{HEP,UIC} - C_{HEP,UEC} \right) \\ & -k_{HEP,uptake} \cdot \frac{C_{HEP,UEC}}{C_{HEP,UEC} + K_{M,HEP,uptake}} \\ & +k_{HEP,efflux} \cdot \frac{C_{HEP,UIC}}{C_{HEP,UIC} + K_{M,HEP,efflux}} \end{aligned} \qquad (1)$$

$$
\begin{aligned}
&V_{HEP,IC} \cdot \frac{dC_{HEP,UIC}}{dt} \\
&= -CL_{HEP,pass} \cdot \left(C_{HEP,UIC} - C_{HEP,UEC}\right) \\
&+ k_{HEP,uptake} \cdot \frac{C_{HEP,UEC}}{C_{HEP,UEC} + K_{M,HEP,uptake}} \\
&- k_{HEP,efflux} \cdot \frac{C_{HEP,UIC}}{C_{HEP,UIC} + K_{M,HEP,efflux}} \\
&- k_{HEP,metabolism} \cdot \frac{C_{HEP,UIC}}{C_{HEP,UIC} + K_{M,HEP,metabolism}} \\
&+ V_{HEP,IC} \cdot k_{off,HEP,IC} \cdot C_{HEP,BIC} \\
&- V_{HEP,IC} \cdot k_{on,HEP,IC} \cdot C_{HEP,UIC} \cdot C_{HEP,AST}
\end{aligned}
\qquad (2)
$$

$$
\frac{dC_{HEP,AST}}{dt} = k_{off,HEP,IC} \cdot C_{HEP,BIC} - k_{on,HEP,IC} \cdot C_{HEP,UIC} \cdot C_{HEP,AST} \qquad (3)
$$

$$
\frac{dC_{HEP.BIC}}{dt} = -k_{off,HEP,IC} \cdot C_{HEP,BIC} + k_{on,HEP,IC} \cdot C_{HEP,UIC} \cdot C_{HEP,AST} \qquad (4)
$$

$V_{HEP,EC}$ and $V_{HEP,IC}$ represent volume of extracellular buffer (0.5 mL per well) and hepatocytes. $V_{HEP,IC}$ is calculated as the product of cell volume per million (0.0026 mL, in-house value), number of cells per cell weight (2.5 million/mg, in-house value), and the cell weight (A_{HEP}) determined in each study. $CL_{HEP,pass}$, $k_{HEP,uptake}$, $k_{HEP,efflux}$, and $k_{HEP,metabolism}$ represent passive diffusion clearance, active uptake, active basal efflux, and metabolic rates. $K_{M,HEP,uptake}$, $K_{M,HEP,efflux}$, and $K_{M,HEP,meta}$ represent Michaelis–Menten constants for uptake, efflux and metabolism. $K_{M,HEP,meta}$ is fixed at values determined from the recombinant CYP assay (Shen et al., 2009) and monkey hepatocyte stability assay. All active rates, $CL_{HEP,pass}$, $K_{M,HEP,uptake}$ and $K_{M,HEP,efflux}$ are estimated by fitting observed experimental data. In the presence of 1 mM inhibitor RSV, all active processes are fixed at zero based on a previous study (Bi et al., 2017). Although RSV is usually used as a transporter inhibitor, in-house data show that at 1 mM, CYP-mediated metabolism is inhibited as well. In SCHH study, we could not detect any accumulation in the bile pocket, consistent with the clinical

DMD Fast Forward. Published on January 12, 2018 as DOI: 10.1124/dmd.117.078808

observation that minimal bosentan parent is identified in the feces following intravenous dosing (Weber et al., 1999); hence the biliary excretion is fixed at zero. $k_{on,HEP,IC}$ and $k_{off,HEP,IC}$ represent the on- and off-rates in intracellular non-specific binding. Given the data we have, $k_{on,HEP,IC}$ and $k_{off,HEP,IC}$ cannot be uniquely identified. As such, $k_{on,HEP,IC}$ value is fixed at a value based on the diffusion (Alberty and Hammes, 1958).

The free fraction of extracellular compound ($f_{u,HEP,EC}$) is calculated as

$$f_{u,HEP,EC} = \frac{1}{1 + K_{a,EC} \cdot A_{HEP} / V_{HEP,EC}} \tag{5}$$

$K_{a,EC}$ is the constant for extracellular non-specific binding. The amount of compound immobilized on the cell surface or plastic plate is assumed as the product of the total amount of extracellular compound and ($1 - f_{u,HEP,EC}$). We assume that the immobilized compound not available for transport, will be mixed with the intracellular compound during cell lysis. In data fitting, the observed compound accumulation in the cell is represented as the sum of bound and unbound intracellular compound and the immobilized extracellular compound. Values of fixed parameters are listed in Table 1, while values of other parameters are estimated by simultaneously fitting data generated with different dosing concentrations under different assay conditions (i.e. with and without transporter inhibitor and calcium).

All the mathematical models presented in this article are implemented in MATLAB 2016a (MathWorks, Natick, MA). The parameter optimization and uncertainty analysis are performed with differential evolution and Markov chain Monte Carlo (MCMC) approaches with details provided in Part 1.

Monkey and rat pharmacokinetic and terminal studies

Monkey pharmacokinetic studies (intravenous bolus) were conducted at the doses of 0.1, 0.33, 1, 3.33, 10, and 20 mg·kg^{-1}. Monkey terminal measurements were performed at 10 mg·kg^{-1}. Rat pharmacokinetic studies (intravenous bolus) were conducted at the doses of 0.1, 0.33, 1, 3.33, and 10 mg·kg^{-1}. Rat terminal measurements were performed at 10 mg·kg^{-1} and with a 3.5 mg·kg^{-1} 4 hour intravenous infusion study. All animal care and in vivo procedures were in accordance with guidelines of the Pfizer Animal Care and Use Committee. Details about methods for animal studies are provided in supplemental materials.

The PBPK model structure developed in Part 1 was used to analyze the animal data. Since only single intravenous escalating doses were modeled, the simulations are not sensitive to the absorption and CYP induction, which were excluded from the final model. The values of physiological parameters are provided in the supplemental materials (Supplemental Table S1). The binding kinetics in plasma and red blood cells (RBC) were estimated using data from *in vitro* assay (Supplemental Figure S1) and a model structure described in Part 1. The passive diffusion clearance between plasma and RBC were determined as described in Part 1. The binding kinetics in the liver tissue is assumed to be the same as that in the hepatocyte uptake assays. Michaelis-Menten constant of hepatic active uptake ($K_{M,liver,uptake}$) for monkey and rat were fixed at values determined from PMH and plated rat hepatocyte (PRH) studies. Michaelis-Menten constant of hepatic metabolism ($K_{M,liver,metabolism}$) for monkey was fixed at a value determined from monkey hepatocyte stability assay, while this parameter for rat was determined by fitting *in vivo* data as *in vitro* data were not available. Parameters with fixed values are listed in Table 2. For both species, Michaelis-Menten constant of hepatic active basal efflux ($K_{M,liver,efflux}$), rates for uptake, metabolism, and basal efflux ($k_{liver,uptake}$, $k_{liver,metabolism}$, $k_{liver,efflux}$), hepatic passive diffusion clearance ($CL_{liver,pass}$), the concentration of endothelin receptors (ET), the ET k_{off} rate, and a scaler for tissue to unbound plasma partition coefficient (Kp_u) are determined by fitting *in vivo* plasma and liver data from various dosing groups simultaneously.

Predicting human systemic and liver pharmacokinetics with in vitro data, animal data, and mechanistic models

For both methods described below, the PBPK model structure and values of fixed parameters for human (including binding parameters and K_M estimated from *in vitro* values) have been provided in Part 1, while values for $CL_{liver,pass}$, $k_{liver,uptake}$, and $k_{liver,metabolism}$ were predicted based on either *in vitro* (Method 1) or animal data (Method 2). The observed systemic exposure following intravenous dosing (Weber et al., 1996; Weber et al., 1999) and deduced liver exposure in Part 1 were used to validate predictions.

Method 1: prediction using human hepatocytes data. The values for $CL_{liver,pass}$, $k_{liver,uptake}$, and $k_{liver,metabolism}$ were predicted using *in vitro* hepatocyte clearance (or rate), physiological IVIVE scaling factors, and empirical IVIVE scaling factors. The physiological IVIVE scaling factor is the number of hepatocytes in the liver. The empirical IVIVE scaling factor is not available for the current model in a prospective prediction. Hence, they are approximated with the published values (Li et al., 2014b). The published binding values in both plasma and liver are generally lower than values used in the current study (e.g., published bosentan plasma free fraction = 0.0053 versus 0.02 in the current study, and published intracellular free fraction = 0.018 versus around 0.036 in the current study). As such, to estimate “ball-park” values in our predictions, the uptake empirical scaling factor is scaled down by 4 fold (from 41 to 10.3), while metabolism and the passive diffusion empirical scaling factor is scaled down by a factor of 2 (i.e. from 0.31 to 0.155, and from 0.29 to 0.145). As a result, $CL_{liver,pass}$ is predicted to be 10.8 uL·min^{-1}·(mg protein)$^{-1}$ × 1 mg protein per million hepatocytes × 120 million hepatocytes per gram liver tissue × 1.69 kg human liver tissue × empirical scaling of 0.145 = 3.17×10^{5} uL·min^{-1} = 19.1 L·hour^{-1}. It is worth noting that although based on current in-house data 1 mg protein is assumed to be 2.5 million hepatocytes in SCHH modeling as described above, here since published empirical scaling factors are used, 1 mg protein is assumed to be 1 million hepatocytes for consistency with the published work (Li et al., 2014b). Essentially the factor of 2.5 million hepatocytes per mg protein is built into the published empirical scaling factors during data fitting. Similarly, values of $k_{liver,uptake}$ and $k_{liver,metabolism}$ are predicted to be 1.20×10^{7} and 4.42×10^{5} nmol·hour^{-1}. The *in vitro* assay cannot provide values about hepatic basal efflux or ET binding, hence they are both ignored from the prediction. Similarly, the *Kp* scaler is assumed to be one.

Method 2: prediction using *in vivo* monkey pharmacokinetic data. The human values for $CL_{liver,pass}$, $k_{liver,uptake}$, and $k_{liver,metabolism}$ are predicted using monkey values (Table 3) scaled by the liver tissue weight difference (0.167 and 1.69 kg for monkey and human liver tissue). For example, human $CL_{liver,pass}$ is predicted to be 4.86 L·hour^{-1} × (1.69 kg / 0.167 kg)$^{\alpha}$ = 49.2 L·hour^{-1}, where α is an allometry exponent. To our knowledge, no similar prediction has been published for a transporter substrate before, hence α is arbitrarily fixed at 1. Similarly, $k_{liver,uptake}$ and $k_{liver,metabolism}$ are predicted to be 6.32×10^{6} and 1.69×10^{6} nmol·hour^{-1}. The hepatic basal efflux process cannot be confidently estimated from monkey *in vivo* data, as such this process is assumed to be zero in human prediction. Human Kp_u scaler and ET binding parameters are assumed to be the same as monkey values (Table 3).

Results

Hepatocyte uptake assay and mechanistic modeling

The observations and simulations for SCHH and PMH assays are provided in Figures 1 and 2. In both SCHH and PMH data analyses, the $k_{HEP,metabolism}$ values are minimal. The active efflux transport process cannot be identified given the current data due to huge uncertainty in estimating $K_{M,HEP,efflux}$. For binding parameters, PMH data are not sufficient to provide confident estimates; hence, we assumed that PMH shared the same binding values as SCHH. All other parameters can be precisely determined (Table 1). For comparison purposes, we also provided the published plated rat hepatocyte rates (Menochet et al., 2012) in Table 1. It is worth noting that although ratios between $k_{HEP,uptake}$ and $K_{M,HEP,uptake}$ are both around 50 for SCHH and PMH, $K_{M,HEP,uptake}$ value is significantly smaller in PMH. In addition, PMH also has a small $CL_{HEP,pass}$ value.

Monkey and rat pharmacokinetic studies and mechanistic modeling

The model can reasonably describe the monkey (Figure 3) and rat (Figure 4) PK data in both plasma and liver samples. All monkey parameters except $k_{liver,efflux}$ and $K_{m,liver,efflux}$ can be confidently estimated (Table 3), a similar phenomenon observed in fitting human data as described in Part 1. The monkey pseudo steady state unbound liver tissue to unbound plasma ratio (Kp_{uu}) and its 95% confidence intervals are 51.3 (39, 70) for 0.1 mg·kg^{-1} dosing, and 66.5 (53, 83) for 20 mg·kg^{-1} dosing. Median liver Kp_{uu} estimates for other dosing groups are between 52.3 and 60.0. In the rat model, parameters for hepatic metabolism and efflux cannot be confidently identified (Table 3). Kp_{uu} and its 95% confidence intervals are 83.4 (16, 130) for 0.1 mg·kg^{-1} dosing, and 87.0 (35, 142) for 10 mg·kg^{-1} dosing.

DMD Fast Forward. Published on January 12, 2018 as DOI: 10.1124/dmd.117.078808
This article has not been copyedited and formatted. The final version may differ from this version.

It is worth noting that if the monkey PK data were not analyzed using the mechanistic model, but with a non-compartment analysis or a traditional two compartment model, the estimated blood clearance would be close to or greater than the blood flow in some dosing groups (Supplemental Table S2), due to ignoring nonlinearity in blood binding and study variabilities.

Prospectively predicting human systemic and liver pharmacokinetics with in vitro data, animal data, and mechanistic models

Both Method 1 (*in vitro* data based) and 2 (monkey data based) provide predictions that largely match the clinical PK data following intravenous dosing, but Method 2 provides a much more reasonable prediction, particularly in the distribution phase (Figure 5). Using predicted hepatic processes from hepatocytes, the predicted human liver Kp_{uu} is 142 for both 10 and 750 mg intravenous dosing (Figure 5). Alternatively, utilizing monkey *in vivo* data predicted hepatic processes, the predicted human Kp_{uu} is 21.1 and 22.9 for 10 and 750 mg intravenous dosing, which are much closer to the value (i.e. 34.9) we estimated with human clinical data in Part 1. The ability to estimate ET binding (particularly *in vivo* concentration of receptor) using Method 2 also contributes to a better systemic prediction (elimination phase), although liver predictions are similar with and without modeling ET binding.

Retrospective analyses on two prediction approaches

In addition to the prospective predictions described above, retrospective analyses were done to better understand IVIVE. In Method 1, the retrospective empirical scaling factors were back-calculated, as the ratios of hepatic processes values estimated in Part 1 using clinical data, to the

DMD Fast Forward. Published on January 12, 2018 as DOI: 10.1124/dmd.117.078808
This article has not been copyedited and formatted. The final version may differ from this version.

physiologically scaled values based on hepatocyte data. The prospective empirical scaling factors we used were about 2-fold greater for $k_{liver,uptake}$ but 1.5 and 2 times lower for $CL_{liver,pass}$ and $k_{liver,metabolism}$ than the retrospective scaling factors (Table 4). Using prospective scaling factors, the over-predicted uptake leads to under-predicted systemic concentration in the distribution phase, while under-predicted metabolism brings the systemic concentration back within the “normal” range during the elimination phase (Figure 5). Although the two mis-predicted processes may cancel each other’s impact upon systemic exposure, both will result in over-predicted liver exposure.

As to Method 1, we also calculated an empirical scaling factor for monkey and rat in retrospective analyses (Table 4) to better understand if different species may have similar empirical scaling for the same compound. Monkey requires different scaling factors from human. Because we cannot confidently estimate *in vivo* $k_{liver,metabolism}$ for rat, only the empirical scaling factors for $CL_{liver,pass}$ and $k_{liver,uptake}$ are provided, and we cannot determine if rat shares the same empirical scaling with human overall.

As to Method 2, even with the allometry exponent (α) arbitrarily fixed at 1, the model reasonably predicts systemic and liver exposure. To understand an α value that best describes the data, a retrospective calculation determined this value to be 0.88. The ratios between values of monkey and human rates are around 0.15 for all three hepatic processes (Table 3), which makes it possible to use the same α across different hepatic processes in consistently translating monkey rates to human based on liver weights. Although human rates of hepatic processes were scaled from monkey *in vivo* values, Michaelis-Menten constants were still fixed at values from human hepatocyte assays. In the absence of *in vitro* hepatocyte data, these constants estimated from monkey *in vivo* data cannot accurately predict human pharmacokinetics (Supplemental Figure S2).

DMD Fast Forward. Published on January 12, 2018 as DOI: 10.1124/dmd.117.078808
This article has not been copyedited and formatted. The final version may differ from this version.

Discussion

Prospectively predicting PK of hepatic transporter substrates in clinical studies remains a challenging task, particularly in predicting liver exposures. Although several approaches have been developed to face this challenge, most focus only on systemic exposure. In addition, due to the use of compound-dependent empirical scaling factors estimated by fitting clinical observation, these published works are more retrospective analyses but rarely tested prospectively. Similarly, when predicting liver-exposure-driven DDI and toxicity of transporter substrates, most published approaches allow floating parameters in order to match clinical observations. Hence, the confidence in using these approaches in real world drug discovery and development is low.

There are two obstacles impeding progress: (1) comprehensive knowledge of human transporter activity, and (2) human liver exposure data to valid prediction approaches developed. The former problem is a result of the latter. Without direct measurement of the liver, researchers can only use indirect surrogates in most studies (e.g., systemic exposure as a surrogate of metabolism, or PK of a victim compound as a surrogate of DDI). Unfortunately, for most compounds, the relationship between the liver exposure and these surrogates is not well understood. Hence, sometimes even a retrospective analysis on clinical observations may not yield a confident result, let alone a prospective prediction.

In this study, we aimed to (1) understand human liver exposure of bosentan, a transporter substrate; and (2) develop and/or validate translational approaches to predict human liver exposure, using currently available preclinical tools. Details about the first goal are provided in Part 1 published in a separate article. Briefly, a deduction approach based on physiological analysis of the observed systemic exposure was used to understand liver exposure in the healthy population. For a

DMD Fast Forward. Published on January 12, 2018 as DOI: 10.1124/dmd.117.078808
This article has not been copyedited and formatted. The final version may differ from this version.

compound with hepatic metabolism like bosentan, the deduction approach seems to currently be the only viable one to predict liver exposure. The two key criteria for such an approach are accuracy and precision: confidence in accuracy resides in the conservation of mass, while the precision is tested with statistical approaches. Unlike most other hepatic transporter substrates, bosentan does not have additional disposition pathways, such as biliary excretion and enterohepatic recirculation, simplifying the problem in analyzing mass conservation through PBPK modeling. Although challenges in modeling bosentan PK exist (e.g., potentially non-linear binding processes), they can still be studied with *in vitro* assays. In addition, there are sufficient clinical data to generate precise parameter estimates and liver predictions, which make bosentan unique from other compounds that have been studied previously (Li et al., 2016). Both advantages help to more confidently establish a relationship among hepatic disposition, exposure, and their systemic surrogate.

In Part 2, several approaches using readily available preclinical tools were tested against the liver exposure deduced in Part 1. Direct liver measurements in terminal animal studies were tested first. Even species with great similarity to human, their liver exposures can be quite different from human's (e.g., Kp_{uu} of about 60 in monkey but about 35 in human for bosentan).

As to mechanistic approaches, although they use the same model structure, and can both describe the systemic exposure, the newly proposed Method 2 (i.e. hepatic processes rates estimated using monkey data) shows a more accurate prediction. As for predicting liver exposure, Method 1 (i.e. hepatic process rates estimated using hepatocyte data) leads to a liver Kp_{uu} of 142, which is substantially greater than the value (34.9) deduced using clinical data. Conversely, Kp_{uu} from Method 2 is more consistent with the deduced value. A set of parameter values that can reasonably simulate systemic exposure or clearance cannot necessarily predict liver exposure due to uncertainty associated with parameter values. Caution should be used when parameter values are estimated by fitting systemic data, and used to simulate liver exposure, or PD, DDI, toxicity driven by it. The details about this topic have been addressed in a previous publication (Li et al., 2016).

In Method 1, the prospective empirical scaling factors leading to over-predicted hepatic uptake were estimated in a previous study by simultaneously fitting human systemic PK of several OATP substrates (Li et al., 2014b). The approach was developed to reduce uncertainty in estimating scaling factors by fitting data of individual compounds. There are multiple reasons that may lead to a mis-match between the current prediction and the old scaling factors. These scaling factors are developed with a model assuming linear kinetics, while the current model uses nonlinear equations to describe both binding and hepatic processes. In addition, *in vitro* SCHH assays were performed with different hepatocyte lots in the two studies, which may have different transporter activity. It should not be concluded that Method 1 is necessarily worse than Method 2 at this time. If the global scaling factor was re-estimated with the current model structure and hepatocyte lots, Method 1 might yield improved systemic and liver predictions. In estimating empirical scaling factors by simultaneously fitting clinical data of several compounds, there are also areas deserving further studies. For example, Kp_u for non-liver tissues are usually fixed at values from *in silico* approaches (Rodgers and Rowland, 2006). The scaling factor estimation can be confounded if non-liver Kp_u is inaccurate for any training compound (Li et al., 2014b; Li et al., 2014c). We have partly tested another topic: for the same compound, can we estimate empirical scaling factor from animal and apply them to human (Watanabe et al., 2009)? Based on our retrospective analysis (Table 4), the values of scaling factors for human and animal can be quite different for compounds like bosentan.

Due to the lack of empirical scaling factors specifically tailored for the current model structure and hepatocyte, we have not fully tested the liver prediction capability of Method 1. From this perspective, Method 2 may be a superior approach since it does not require data from other training compounds, although its prediction accuracy should be further validated with additional compounds in future. Method 2 requires data from both *in vivo* monkey studies (for hepatic process rates) and *in vitro* studies (for Michaelis-Menten constants). We have tested prediction without *in vitro* data, where both rates and Michaelis-Menten constants are estimated using *in vivo* monkey data. However, the systemic exposure is under-predicted while liver exposure is over-predicted. A similar phenomenon has been published previously with another acidic compound with a molecular weight of 428 (i.e. a potential OATP substrate), GSK269984A. Although rates may be similar between two species, monkey may have a smaller $K_{M,liver,uptake}$ value than human, which may cause over-predicted uptake. Hence, unless it has been proven that the compounds have large enough K_M values in both monkey and human, hepatic processes estimated from monkey *in vivo* data per se should not be used to predict human PK without accounting for species K_M difference. We have also tried to use Method 2 but with hepatic rates, Kp_u scaler and ET binding parameters estimated from rat in vivo data. An allometry exponent of 0.8 seems to best describe the human data, however the simulation still over-predicts liver exposure but under-predictes systemic exposure (Supplemental Figure S3). It worth noting that we do not have confidently estimated Michaelis-Menten constants from in vitro assays for rat, hence the estimated rat in vivo hepatic rates and potentially other fitted rat parameters are not confident either, which may contribute to the mis-prediction.

In conclusion, using bosentan data, we have provided an example for prospectively predicting hepatic exposure of a transporter substrate. The accuracies of the new and previously established approaches have been validated against the human liver Kp_{uu} deduced in Part 1. The new approach shows the highest accuracy in this study.

Ethical approval

All animal care and in vivo procedures were in accordance with guidelines of the Pfizer Animal Care and Use Committee.

Acknowledgement

We thank Dr. Manthena V. Varma (Pfizer Inc.) for helpful discussions, and Ms. Karen Atkinson (Pfizer Inc.) for assistance with manuscript editing.

Authorship Contributions

Participated in research design: Li, Kimoto, Niosi, Tess, Lin, Tremaine, and Di.

Conducted experiments: Kimoto, Niosi, and Lin.

Contributed new reagents or analytic tools: Li.

Performed data analysis: Li, Kimoto, Niosi, Tess, Lin, Tremaine, and Di.

Wrote or contributed to the writing of the manuscript: Li, Kimoto, Niosi, Lin, and Di.

References

Alberty RA and Hammes GG (1958) Application of the Theory of Diffusion-controlled Reactions to Enzyme Kinetics. *The Journal of Physical Chemistry* **62:**154-159.

Bi YA, Scialis RJ, Lazzaro S, Mathialagan S, Kimoto E, Keefer J, Zhang H, Vildhede AM, Costales C, Rodrigues AD, Tremaine LM, and Varma MVS (2017) Reliable Rate Measurements for Active and Passive Hepatic Uptake Using Plated Human Hepatocytes. *AAPS J* **19:**787-796.

Li R, Barton HA, and Varma MV (2014a) Prediction of pharmacokinetics and drug-drug interactions when hepatic transporters are involved. *Clin Pharmacokinet* **53:**659-678.

Li R, Barton HA, Yates PD, Ghosh A, Wolford AC, Riccardi KA, and Maurer TS (2014b) A "middle-out" approach to human pharmacokinetic predictions for OATP substrates using physiologically-based pharmacokinetic modeling. *J Pharmacokinet Pharmacodyn* **41:**197-209.

Li R, Ghosh A, Maurer TS, Kimoto E, and Barton HA (2014c) Physiologically based pharmacokinetic prediction of telmisartan in human. *Drug Metab Dispos* **42:**1646-1655.

Li R, Maurer TS, Sweeney K, and Barton HA (2016) Does the Systemic Plasma Profile Inform the Liver Profile? Analysis Using a Physiologically Based Pharmacokinetic Model and Individual Compounds. *AAPS J* **18:**746-756.

Menochet K, Kenworthy KE, Houston JB, and Galetin A (2012) Simultaneous assessment of uptake and metabolism in rat hepatocytes: a comprehensive mechanistic model. *J Pharmacol Exp Ther* **341:**2-15.

Morse BL, Cai H, MacGuire JG, Fox M, Zhang L, Zhang Y, Gu X, Shen H, Dierks EA, Su H, Luk CE, Marathe P, Shu YZ, Humphreys WG, and Lai Y (2015) Rosuvastatin Liver Partitioning in Cynomolgus Monkeys: Measurement In Vivo and Prediction Using In Vitro Monkey Hepatocyte Uptake. *Drug Metab Dispos* **43:**1788-1794.

Rodgers T and Rowland M (2006) Physiologically based pharmacokinetic modelling 2: predicting the tissue distribution of acids, very weak bases, neutrals and zwitterions. *J Pharm Sci* **95:**1238-1257.

Shen G, Yao M, Fura A, and Zhu M (2009) In vitro metabolite identification and cytochrome P450 reaction phenotyping of Bosentan, a dual endothelin receptor antagonist, in: *AAPS Annual Meeting and Exposition*, Los Angeles, CA, US.

Shimizu K, Takashima T, Yamane T, Sasaki M, Kageyama H, Hashizume Y, Maeda K, Sugiyama Y, Watanabe Y, and Senda M (2012) Whole-body distribution and radiation dosimetry of [11C]telmisartan as a biomarker for hepatic organic anion transporting polypeptide (OATP) 1B3. *Nucl Med Biol* **39:**847-853.

Watanabe T, Kusuhara H, Maeda K, Shitara Y, and Sugiyama Y (2009) Physiologically based pharmacokinetic modeling to predict transporter-mediated clearance and distribution of pravastatin in humans. *J Pharmacol Exp Ther* **328:**652-662.

Weber C, Gasser R, and Hopfgartner G (1999) Absorption, excretion, and metabolism of the endothelin receptor antagonist bosentan in healthy male subjects. *Drug Metab Dispos* **27:**810-815.

Weber C, Schmitt R, Birnboeck H, Hopfgartner G, van Marle SP, Peeters PA, Jonkman JH, and Jones CR (1996) Pharmacokinetics and pharmacodynamics of the endothelin-receptor antagonist bosentan in healthy human subjects. *Clin Pharmacol Ther* **60:**124-137.

Figure Captions

Figure 1. Observed and simulated intracellular accumulation of bosentan in sandwich cultured human hepatocyte assays. Each subplot represents a different dosing group. Red, blue, and black represent three different conditions: control, with 1 mM RSV, and without calcium. The solid lines and markers represent simulations and data. Both horizontal and vertical axes are in log scale.

Figure 2. Observed and simulated intracellular accumulation of bosentan in plated monkey hepatocyte assays. Each subplot represents a different dosing group. Red and blue represent two different conditions: without and with 1 mM RSV. The solid lines and markers represent simulations and data. Both horizontal and vertical axes are in log scale.

Figure 3. Observed and simulated monkey pharmacokinetic time courses. Red and blue indicates total plasma and total liver concentrations. The markers, solid line, and shaded areas represent the data, median simulations, and 95% confidence intervals generate with parameter values identified in Markov chain Monte Carlo.

Figure 4. Observed and simulated rat pharmacokinetic time courses. Red and blue indicates total plasma and total liver concentrations. The markers, solid line, and shaded areas represent the data, median simulations, and 95% confidence intervals generate with parameter values identified in Markov chain Monte Carlo.

Figure 5. Prospectively predicted systemic pharmacokinetics of bosentan, and its unbound liver to unbound plasma ratio. The dashed and solid lines represent prediction based on *in vitro* data (Method 1) and monkey *in vivo* data (Method 2). Markers represent clinical observation. Red and blue represent total systemic concentration (left axis) and unbound liver to unbound plasma ratio (right axis).

Table 1. Median and 95% confidence interval of estimated parameters in sandwich cultured human hepatocytes (SCHH) model and plated monkey hepatocytes (PMH) model, and published parameter values in plated rat hepatocytes (PRH) model.

Parameters	Units	SCHH	PMH	PRH
$CL_{HEP,pass}$	$uL \cdot min^{-1} \cdot mg^{-1}$	10.8 (9.7, 12)	3.55 (2.2, 5.3)	13.5
$k_{HEP,uptake}$	$pmol \cdot min^{-1} \cdot mg^{-1}$	96.3 (67, 140)	24.6 (15, 39)	488
$K_{M,HEP,uptake}$	nM	4340 (2800, 6800)	1280 (800, 2000)	6400
$k_{HEP,efflux}$	$pmol \cdot min^{-1} \cdot mg^{-1}$	0.117 (0.084, 0.15)	68.5 (25, 170)	
$K_{M,HEP,efflux}$	nM	0.0100	7100 (2400, 2.1×10^{4})	
$k_{HEP,metabolism}$	$pmol \cdot min^{-1} \cdot mg^{-1}$	3.08×10^{-8}	5.90×10^{-9}	
$K_{M,HEP,metabolism}$	nM	6.9×10^{4} (fixed)	2.85×10^{4} (fixed)	
$k_{on,HEP,IC}$	$nM^{-1} \cdot min^{-1}$	60 (fixed)	60 (fixed)	
$k_{off,HEP,IC}$	min^{-1}	8.45×10^{5} (5.8×10^{5}, 1.2×10^{6})	8.45×10^{5} (fixed)	
Total intracellular binding site	nM	3.82×10^{5} (3.1×10^{5}, 4.7×10^{5})	3.82×10^{5} (fixed)	
$K_{a,EC}$	$mL \cdot mg^{-1}$	2.75×10^{-3} (1.8×10^{-3}, 3.7×10^{-3})	0.0163 (0.0133, 0.0194)	
Cell number	million cells per mg measured protein	2.5 (fixed)	2.5 (fixed)	
Cell volume	mL per million cells	2.6×10^{-3} (fixed)	2.6×10^{-3} (fixed)	
$V_{HEP,EC}$	mL per well	0.5 (fixed)	0.5 (fixed)	

PRH data are published in a previous study (Menochet et al., 2012). Median and confidence interval are not provided for the parameters with high uncertainty (i.e. the range of approximated confidence interval is greater than 20 magnitude). The globally optimized value is provided instead.

DMD Fast Forward. Published on January 12, 2018 as DOI: 10.1124/dmd.117.078808

Table 2. Values of fixed parameters in monkey and rat physiologically based pharmacokinetic models.

Parameter	Unit	Monkey	Source	Rat	Source
pKa		5.2 (acidic)	In-house	5.2 (acidic)	In-house
$logD_{7.4}$		1.3	In-house	1.3	In-house
MW	$g \cdot mol^{-1}$	551.6	In-house	551.6	In-house
$K_{M,liver,uptake}$	nM	1280	PMH	6400	PRH (Menochet et al., 2012)
$K_{M,liver,metabolism}$	nM	2.85×10^4	Suspended monkey hepatocyte		
k_{on}	$nmol^{-1} \cdot hour^{-1}$	3600	(Alberty and Hammes, 1958)	3600	(Alberty and Hammes, 1958)
$k_{off,plasma}$	$hour^{-1}$	2.41×10^8	Supplemental materials	5.88×10^7	Supplemental materials
$k_{off,RBC}$	$hour^{-1}$	7.29×10^5	Supplemental materials	5.00×10^6	Supplemental materials
$k_{off,liver,tissue}$	$hour^{-1}$	4.80×10^7	SCHH	4.80×10^7	SCHH
Binding site in plasma	nM	1.47×10^6	Supplemental materials	1.02×10^6	Supplemental materials
Binding site in RBC	nM	1.10×10^4	Supplemental materials	3.35×10^4	Supplemental materials
Binding site liver tissue	nM	3.82×10^5	SCHH	3.82×10^5	SCHH
HCT		0.431	In-house	0.540	In-house
$CL_{systemic,blood,pass}$	$L \cdot hour^{-1}$	41.7	As described in Part 1	3.94	As described in Part 1
$CL_{liver,blood,pass}$	$L \cdot hour^{-1}$	3.89	As described in Part 1	0.591	As described in Part 1

Table 3. Mean and 95% confidence interval of parameters in human, monkey and rat physiologically based pharmacokinetic models estimated by fitting *in vivo* data, and retrospective ratios among different species.

		Human	Monkey	Rat	Monkey to human ratio	Rat to human ratio
ET k_{off}	hour^{-1}	1.61×10^{4} $(7200, 3.4\times10^{4})$	1039 $(240, 1.1\times10^{4})$	47.9 (4.78, 505)	0.0645	2.98×10^{-3}
ET total concentration	nM	2750 (1400, 4900)	2310 (1400, 4100)	2251 (968, 3890)	0.840	0.819
$CL_{liver,pass}$	L·hour^{-1}	23.9 (13, 44)	4.86 (2.8, 8.5)	0.0322 $(8.98\times10^{-4}, 0.619)$	0.203	1.35×10^{-3}
$k_{liver,uptake}$	nmol·hour^{-1}	4.78×10^{6} $(3.8\times10^{6}, 6.5\times10^{6})$	6.25×10^{5} $(4.6\times10^{5}, 9.0\times10^{5})$	1.12×10^{5} $(8.9\times10^{4}, 3.4\times10^{5})$	0.131	0.0234
$k_{liver,metabolism}$	nmol·hour^{-1}	1.00×10^{6} $(8.0\times10^{5}, 1.3\times10^{6})$	1.67×10^{5} $(1.5\times10^{5}, 1.8\times10^{5})$	1.50×10^{3}	0.167	
$k_{liver,efflux}$	nmol·hour^{-1}	6.00×10^{4}	0.539	5.55		
$K_{m,liver,efflux}$	nM	1.48×10^{6}	3.5×10^{4}	93.9		
Non-liver tissue Kp_u scaler		1 (fixed)	1.47 (0.86, 2.3)	4.53 (< 7.11)	1.47	4.53
Body weight	kg	70.0 (fixed)	6.20 (fixed)	0.250 (fixed)	0.0886	3.57×10^{-3}
Liver tissue weight	kg	1.69 (fixed)	0.167 (fixed)	0.0103 (fixed)	0.0988	6.09×10^{-3}

1. Median and confidence interval are not provided for the parameters with high uncertainty (i.e. the range of approximated confidence interval is greater than 20 magnitude). The globally optimized value is provided instead.
2. The values for human are generated in Part 1 published in a separated article; while values for rat and monkey are estimated in the current study.
3. Because $K_{m,liver,metabolism}$ for rat is not available from *in vitro* studies, it is estimated by fitting *in vivo* pharmacokinetic data with other parameters. The mean is estimated to be 6430 nM but with a high uncertainty.

Table 4. Physiologically scaled *in vivo* hepatic clearance processes based on hepatocyte data, and *in vitro* to *in vivo* extrapolation (IVIVE) empirical scaling factor (ESF).

		Human	Monkey	Rat
Physiologically scaled $CL_{liver,pass}$	$L \cdot hour^{-1}$	131	5.10	0.901
Prospective diffusion ESF		0.145		
Retrospective diffusion ESF		0.182	0.953	0.0357
Physiologically scaled $k_{liver,uptake}$	$nmol \cdot hour^{-1}$	1.17×10^6	3.53×10^4	3.26×10^4
Prospective uptake ESF		10.3		
Retrospective uptake ESF		4.08	17.7	3.96
Physiologically scaled $k_{liver,metabolism}$	$nmol \cdot hour^{-1}$	2.85×10^6	1.15×10^4	
Prospective metabolism ESF		0.155		
Retrospective metabolism ESF		0.351	0.146	

1. Hepatic transport processes are predicted with SCHH, while metabolic rates are predicted with suspended hepatocytes (*in vitro* metabolic rates: human hepatocytes, 234.6 $pmol \cdot min^{-1} \cdot million^{-1}$; monkey hepatocytes, 798 $pmol \cdot min^{-1} \cdot million^{-1}$).
2. $CL_{liver,pass}$, $k_{liver,uptake}$, and $k_{liver,metabolism}$ provided in this table is calculated as the product of hepatocyte clearance (or rate, Table 1) and physiological scaling factors (i.e. tissue weight and HPPGL), without ESF. HPPGL represents hepatocytes per gram of liver, which is 120, 122, and 108 million for human, monkey, and rat.
3. Prospective ESF is approximated using published values after accounting for different binding values between publication and the current study (see details in the method section).
4. Retrospective ESF is calculated as the ratio of clearance (or rate) estimated by fitting *in vivo* data (Table 3) to the physiologically predicted clearance (or rate) in this table.
5. For rat, we only provide IVIVE ratio for uptake, due to high uncertainty associated with other parameters in fitting rat *in vivo* data.

Figure 1.

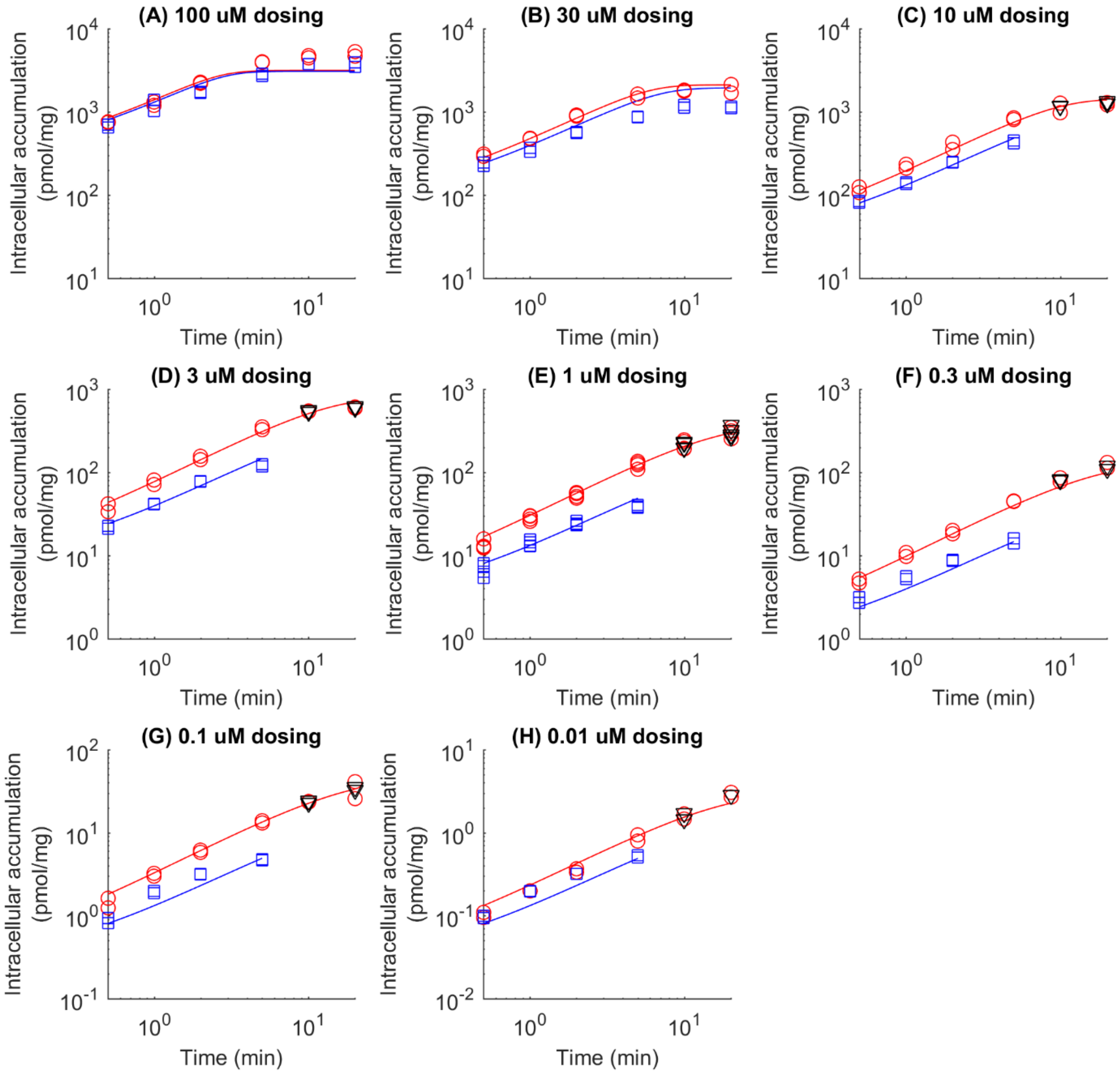
(A) 100 uM dosing
(B) 30 uM dosing
(C) 10 uM dosing
(D) 3 uM dosing
(E) 1 uM dosing
(F) 0.3 uM dosing
(G) 0.1 uM dosing
(H) 0.01 uM dosing
Intracellular accumulation (pmol/mg)
Time (min)
10^{4}
10^{3}
10^{2}
10^{1}
10^{0}
10^{-1}
10^{-2}

DMD Fast Forward. Published on January 12, 2018 as DOI: 10.1124/dmd.117.078808
This article has not been copyedited and formatted. The final version may differ from this version.

Figure 2.

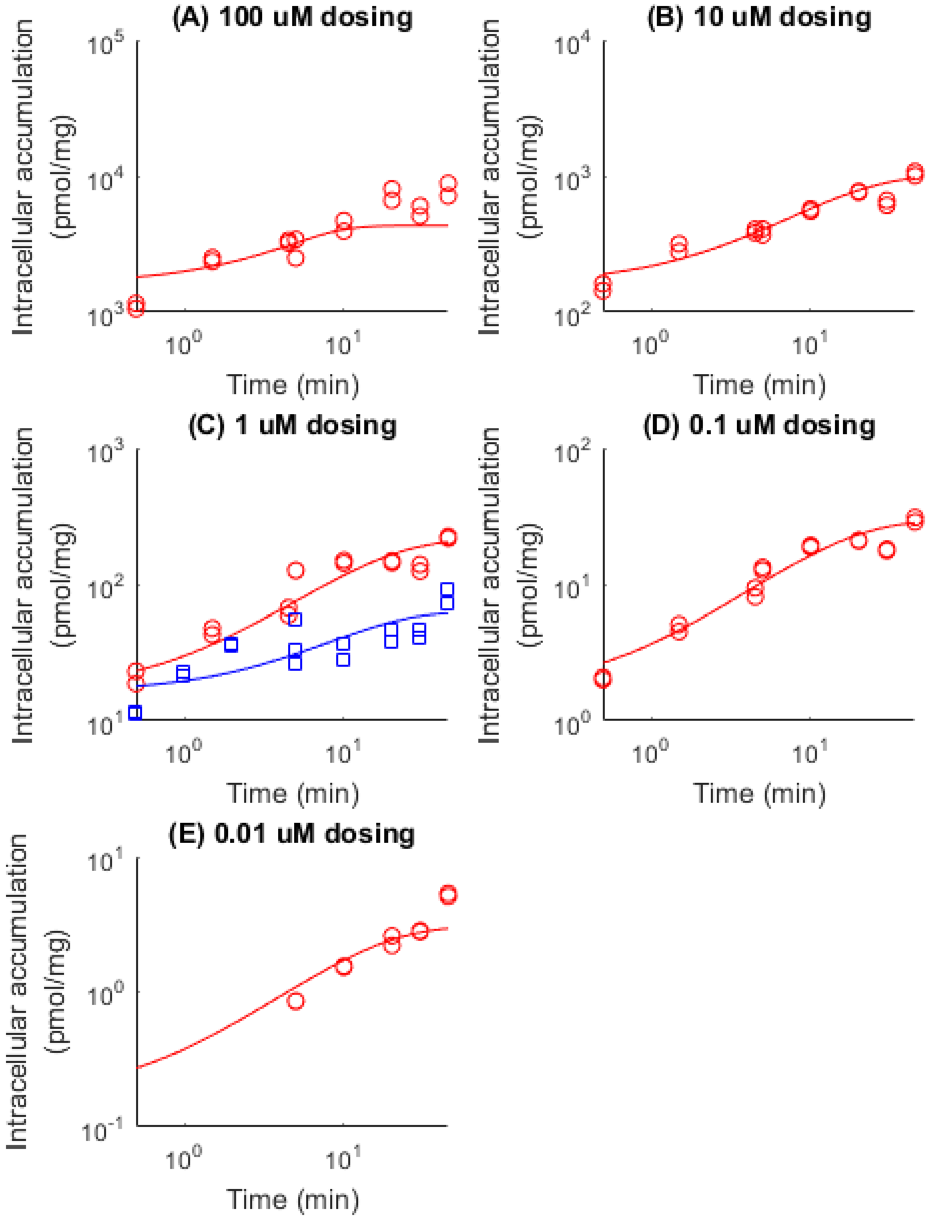

DMD Fast Forward. Published on January 12, 2018 as DOI: 10.1124/dmd.117.078808

Figure 3.

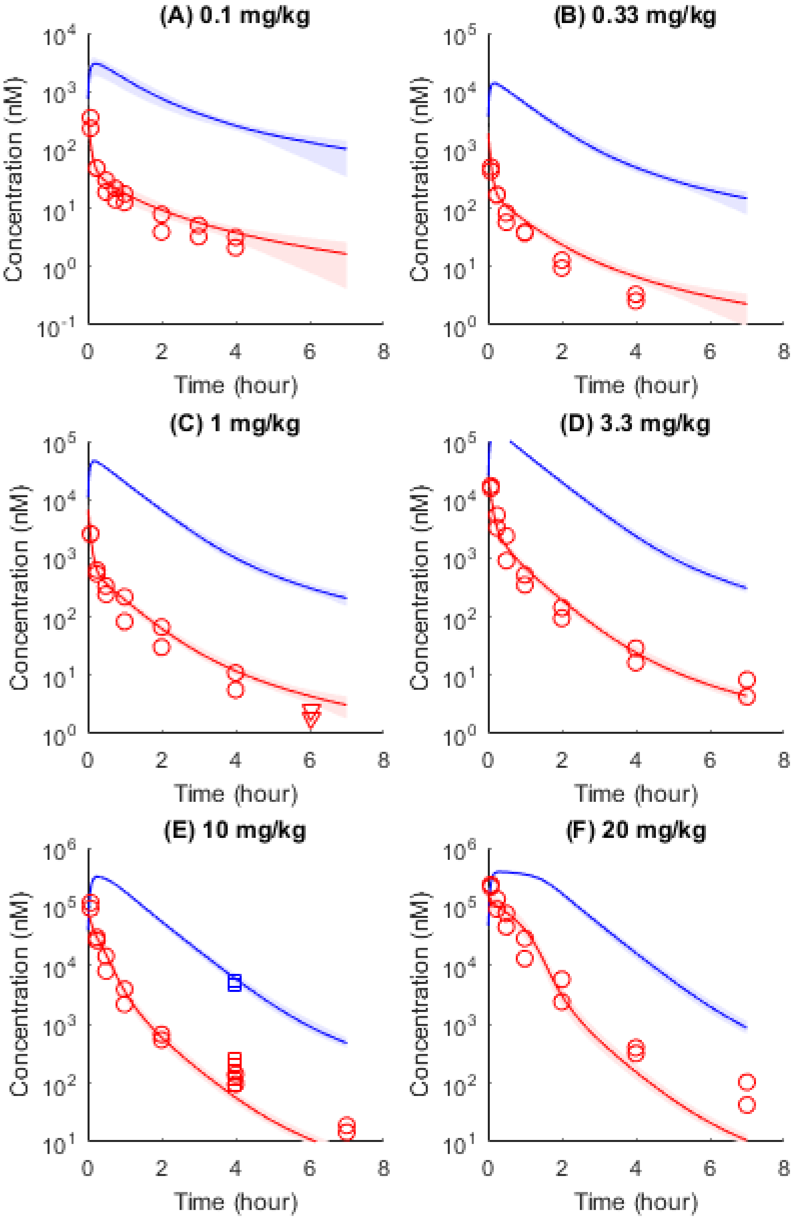

Figure 4.

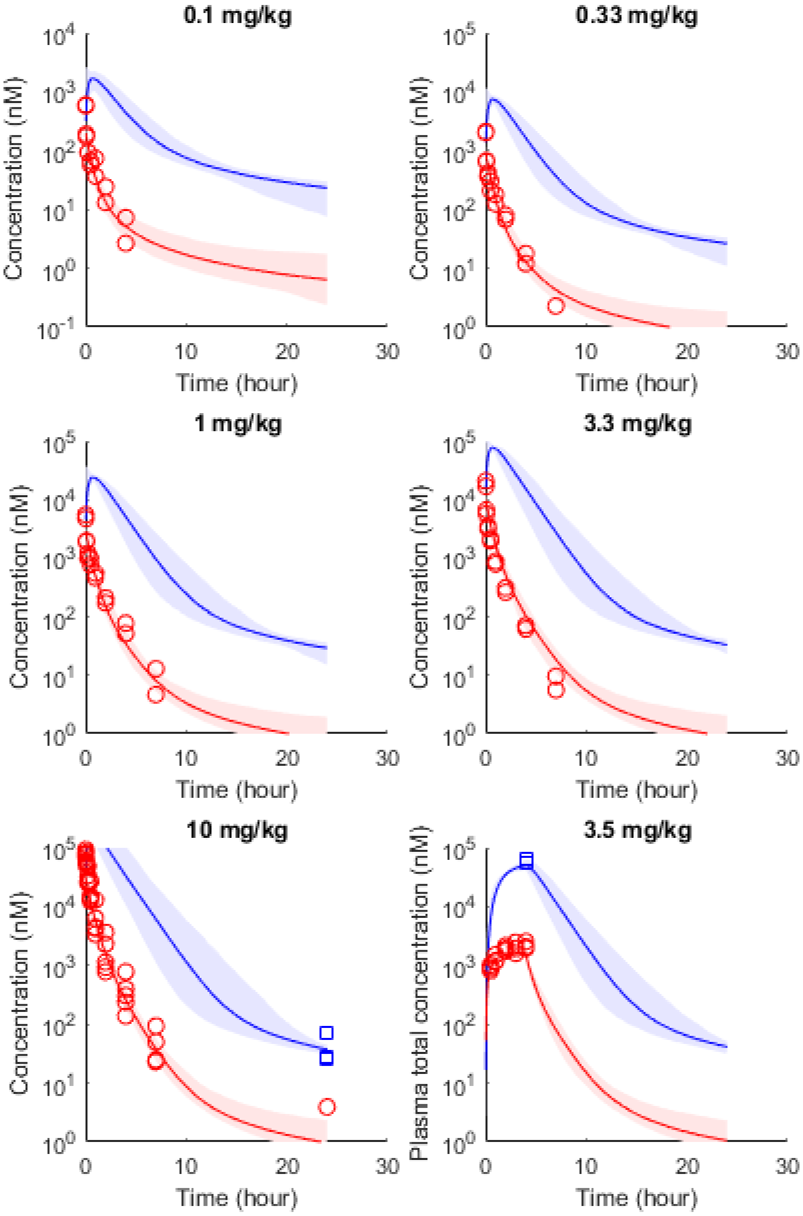
0.1 mg/kg
0.33 mg/kg
1 mg/kg
3.3 mg/kg
10 mg/kg
3.5 mg/kg
Concentration (nM)
Plasma total concentration (nM)
Time (hour)
10^{-1}
10^{0}
10^{1}
10^{2}
10^{3}
10^{4}
10^{5}
0
10
20
30

Figure 5.

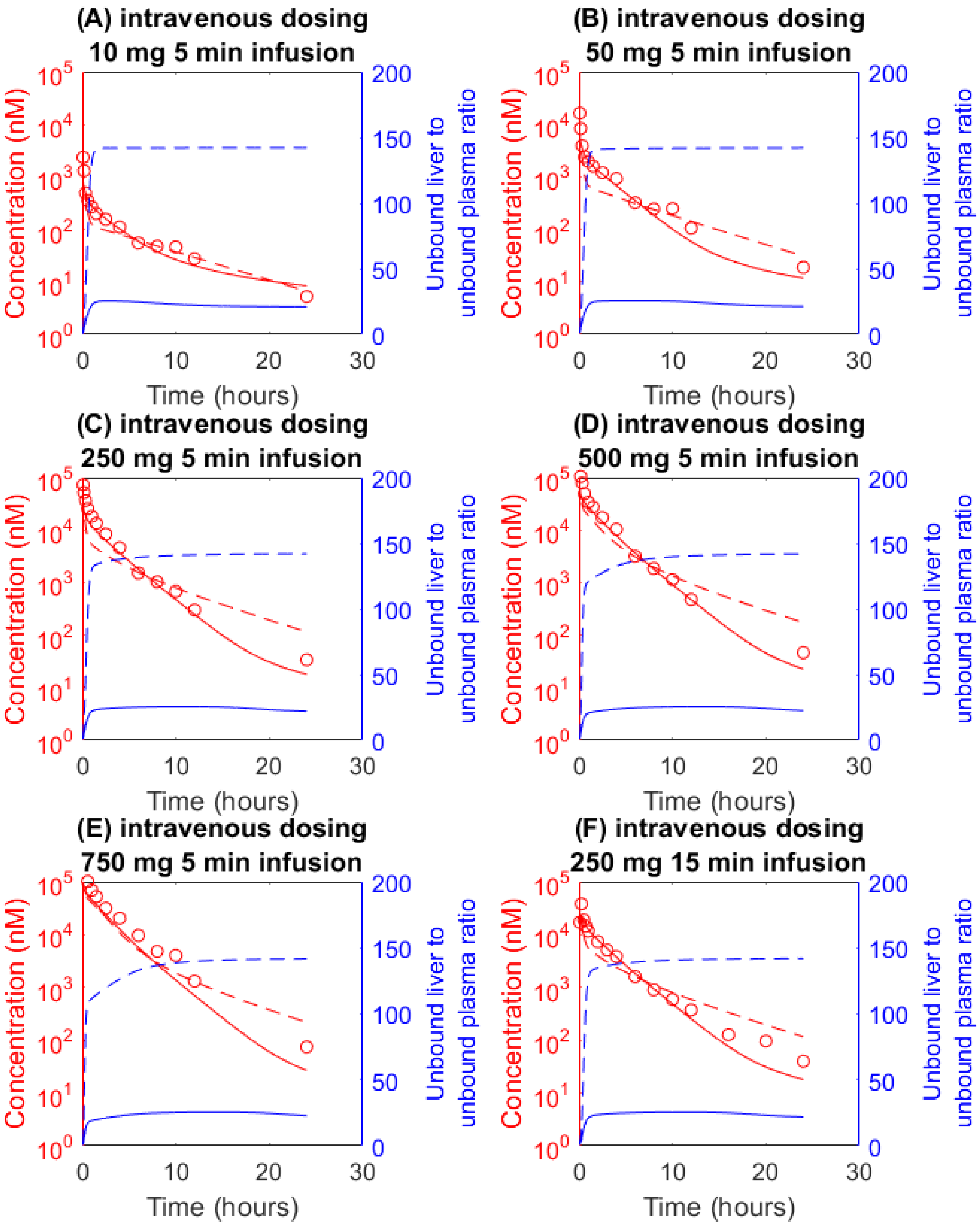
(A) intravenous dosing
10 mg 5 min infusion
(B) intravenous dosing
50 mg 5 min infusion
(C) intravenous dosing
250 mg 5 min infusion
(D) intravenous dosing
500 mg 5 min infusion
(E) intravenous dosing
750 mg 5 min infusion
(F) intravenous dosing
250 mg 15 min infusion
Concentration (nM)
10^0
10^1
10^2
10^3
10^4
10^5
Unbound liver to unbound plasma ratio
0
50
100
150
200
Time (hours)
0
10
20
30

DRUG METABOLISM AND DISPOSITION

Supplemental Materials

A study on pharmacokinetics of bosentan with systems modeling, Part 2: prospectively predicting systemic and liver exposure in healthy subjects

Rui Li, Emi Kimoto, Mark Niosi, David A. Tess, Jian Lin, Larry M. Tremaine, Li Di

Figure S1. Observed and fitted plasma free fraction and blood to plasma ratio of rat, monkey, and human. Human plasma free fraction data are digitized from a previous publication [1], while human blood to plasma ratio are published in Part 1.

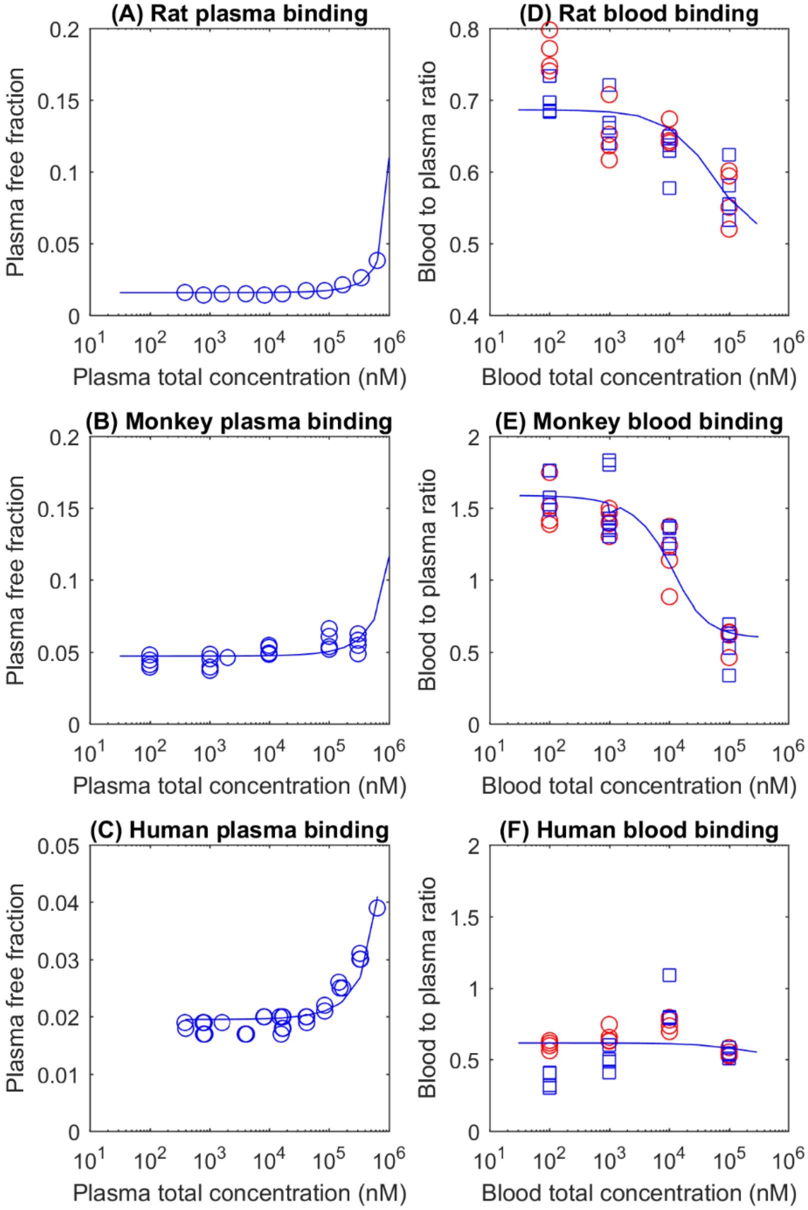

Figure S2. Predicted human systemic exposure (red) and unbound liver to unbound plasma ratio (blue). The parameter values are generated by scaling monkey parameter values with ratios of liver tissue weights between human and monkey, while monkey parameter (including $K_{m,liver,uptake}$ and $K_{m,liver,metabolism}$) values are estimated by fitting in vivo pharmacokinetic data. The markers, solid line, and shaded areas represent the data, median simulations, and 95% intervals generate with parameter values identified in Markov chain Monte Carlo.

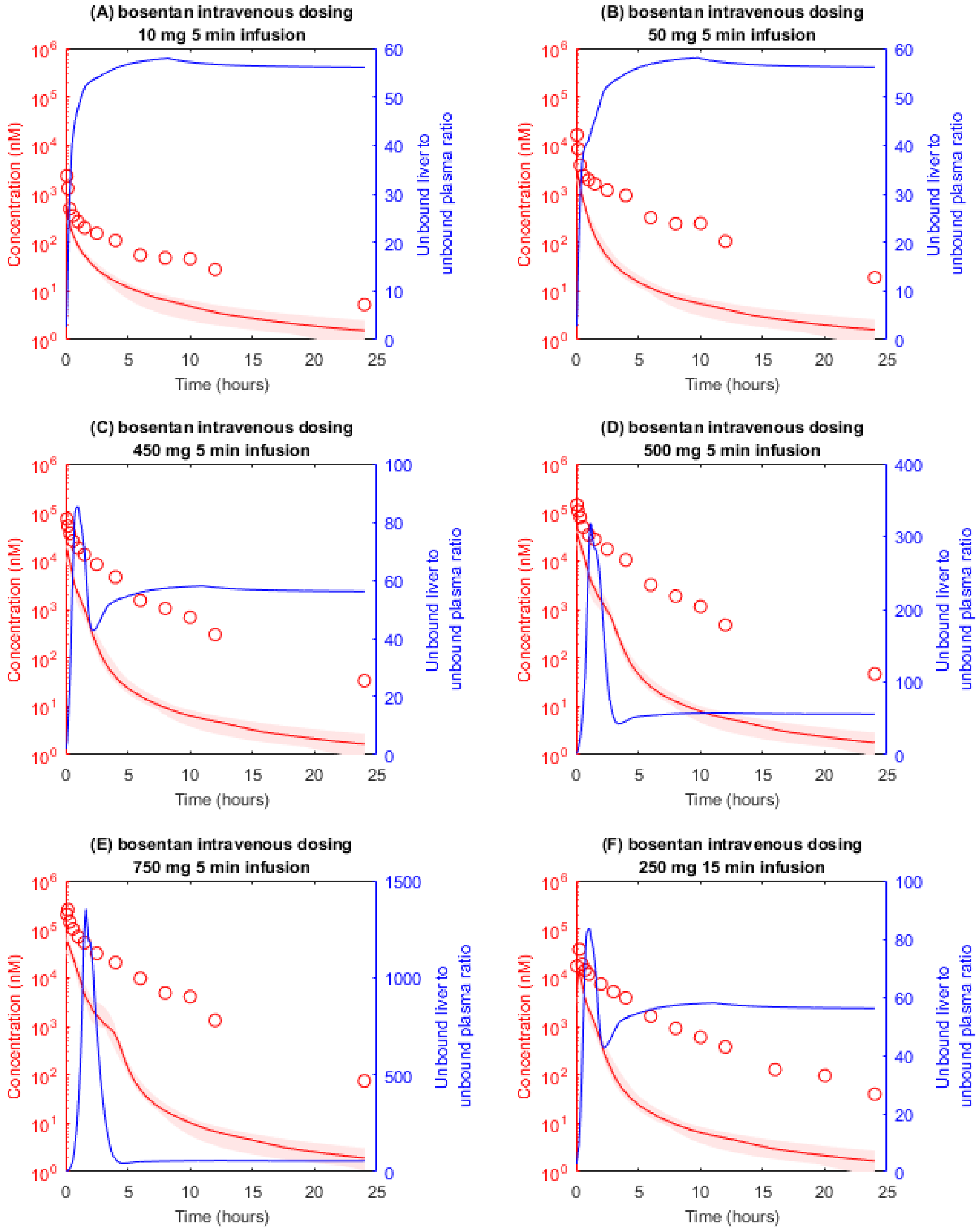

Figure S3. Predicted human systemic exposure (red) and unbound liver to unbound plasma ratio (blue). The parameter values are generated by scaling rat parameter values with ratios of liver tissue weights between human and rat, while rat parameter (including $K_{m,liver,metabolism}$) values are estimated by fitting in vivo pharmacokinetic data. The markers and solid line represent the data and simulations.

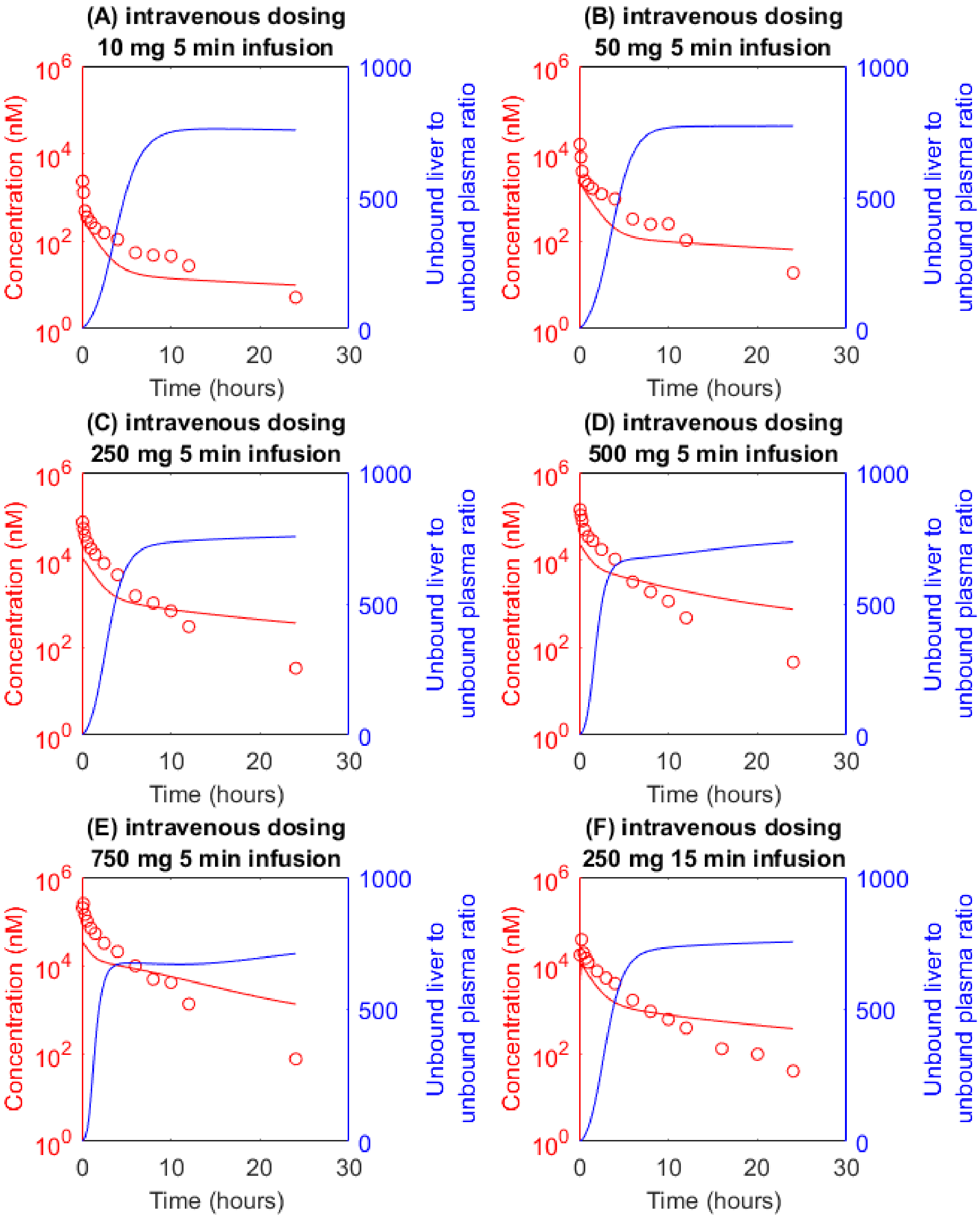

Table S1. Values for physiological parameters [1].

Tissue	Blood flow (L·hour^{-1}·kg^{-1})			Volume (L·kg^{-1})		
	Cynomolgus Monkey	**SD Rat**	**Human**	**Cynomolgus Monkey**	**SD Rat**	**Human**
Adipose	0.24	0.0960	0.222	0.130	0.04	0.143
Bone	0.612	0.607	0.216	0.0632	0.0632	0.124
Brain	0.864	0.319	0.6	0.019	0.0068	0.0207
Gut [2]	1.42	2.90	0.558	0.0504	0.0444	0.0258
Villi blood [3]	0.204	0.710	0.256			0.000157
Heart	0.72	0.941	0.128	0.0034	0.0032	0.0038
Kidney	1.66	2.21	0.942	0.006	0.0092	0.0044
Liver blood (arterial) [4]	0.610	0.648	0.266	0.00466	0.00871	0.00468
Liver tissue	-	-	-	0.027	0.0412	0.0241
Muscle	1.08	1.80	0.642	0.5	0.488	0.429
Pancreas	0.122	0.240	0.114	0.0052	0.0052	0.0012
Skin	0.648	1.20	0.258	0.1	0.160	0.111
Spleen	0.252	0.300	0.066	0.0017	0.0024	0.0027
Systemic blood [5]	-	-	-	0.0629	0.0589	0.0723
Remaining [6]	0.102	0.229	0.0024	0.0205	0.0596	0.0288
Total [7]	8.53	12.2	4.26	1	1	1

1. All the values (except for those noted below) are calculated based on a previous publication [2].

2. The gut volume is calculated as the sum of the reported values for gut and stomach. Its blood flow is the sum of the reported values for gut and stomach minus villi blood flow.
3. Human villi blood flow is reported by [3], while animal values are acquired from Simcyp Version 16 (Certara USA, Inc., Princeton, NJ, USA). Shah and Betts reported the small intestine blood volume as 0.000157 $L \cdot kg^{-1}$ [4]. We assume that this volume is the same as villi blood volume.
4. The arterial liver blood flows are calculated by removing gut, pancreas, and spleen values from reported liver values. Shah and Betts report the liver blood volumes [4].
5. The systemic blood volumes are the sums of the reported venous and arterial volumes minus liver blood volumes. HCT values (0.43 for monkey, 0.54 for rat, and 0.52 for human) are determined experimentally to separate blood volumes into RBC and plasma volumes.
6. The values for the rest of body are calculated to keep the mass balance.
7. The total blood flows (i.e. cardiac outputs) are the reported lung blood flows for monkey and rat, and the sum of all report blood flows excluding lung for human.

Table S2. Systemic clearances and volume of distributions of monkey pharmacokinetic data. The data are analyzed using a two compartment pharmacokinetic model, while the parameters are quantified with the Markov Chain Monte Carlo method.

MCMC of a two compartment PK model (median and 95% confidence intervals)

	Parameters of two compartment model					Trapezoid of simulations	
Dosing amount	CL	Q	V1	V2	Total V	CL	Vd$_{ss}$
mg·kg^{-1}	L·hour^{-1}·kg^{-1}	L·hour^{-1}·kg^{-1}	L·kg^{-1}	L·kg^{-1}	L·kg^{-1}	L·hour^{-1}·kg^{-1}	L·kg^{-1}
0.1	1.85 (0.37, 2.4)	1.23 (0.037, 2.4)	0.244 (0.0066, 0.58)	1.18 (0.047, 2.1)	1.44 (0.054, 2.5)	1.85 (0.37, 2.4)	1.45 (0.057, 2.5)
0.33	3.24 (2.6, 3.9)	1.90 (0.89, 3.6)	0.81 (0.45, 1.6)	1.3 (0.91, 2.0)	2.19 (1.5, 3.3)	3.24 (2.6, 3.9)	2.22 (1.6, 3.3)
1	2.18 (0.28, 3.6)	1.12 (1.5×10^{-7}, 6100)	0.426 (0.046, 3.0)	0.75 (8.5×10^{-8},47000)	1.29 (0.35, 47000)	2.22 (0.45, 3.6)	1.32 (0.32, 110)
3.3	1.45 (0.93, 2.1)	0.178 (0.062, 0.53)	0.337 (0.14, 0.81)	0.268 (0.11, 0.95)	0.616 (0.30, 1.9)	1.45 (0.93, 2.1)	0.628 (0.31, 1.9)
10	0.667 (0.42, 0.93)	0.0663 (0.019, 0.17)	0.159 (0.075, 0.31)	0.0814 (0.034, 0.18)	0.245 (0.13, 0.46)	0.667 (0.42, 0.93)	0.250 (0.13, 0.47)
20	0.332 (6.5×10^{-9}, 0.54)	0.0341 (0.0018, 0.51)	0.210 (0.101, 0.402)	0.154 (0.0045, 920)	0.453 (0.13, 920)	0.332 (1.3×10^{-5}, 0.54)	0.449 (0.14, 900)

Method for plated monkey hepatocyte (MPH) studies

Materials and Reagents. In VitroGro-HT (thawing), In VitroGro-CP (plating), and In VitroGro-HI (incubation) hepatocyte media were purchased from BioreclamationIVT (Baltimore, MD). Hanks balanced salt solution (HBSS) - Ca2+/Mg2+-containing - was purchased from Lonza (Walkersville, MD). BioCoat 24-well plates and Matrigel were purchased from Corning (Kennebunk, ME). The BCA Protein Assay Kit was purchased from PierceBiotechnology (Rockford, IL). HPLC grade methanol (MeOH), acetonitrile, and water were obtained from Fisher Chemical (Fair Lawn, NJ). Bosentan was purchased from Sequoia Research Products (Pangbourne, UK). Formic acid, Dulbecco's phosphate-buffered saline, and all other chemicals were purchased from Sigma (St. Louis, MO). Cryopreserved monkey hepatocytes (cynomolgus, female, lot 10106012) were purchased from In Vitro ADMET, (Columbia, MD).

Plated Monkey Hepatocytes (PMH). Plateable cryopreserved hepatocytes were thawed and plated as described previously for plated human hepatocytes [5]. Briefly, hepatocytes were thawed in a water bath at 37°C and placed on ice. The cells were then poured into In VitroGro-HT medium at 37°C at a ratio of one vial/50 mL in a conical tube. The cells were centrifuged at 50 × g for 3 minutes and resuspended at 0.75×10^6 cells/mL in In VitroGro-CP medium. Cell viability was determined by trypan blue exclusion. Hepatocyte suspensions were plated in collagen-coated 24-well plates at a density of 0.375×10^6 cells/well in a volume of 0.5 mL/well. After 6 hours of incubation at 37°C, uptake study was conducted.

Determination of Uptake in PMH. Uptake of bosentan was measured in PMH. The hepatocytes were first rinsed twice with HBSS and then pre-incubated for 10 minutes with HBSS in the absence or presence of 1 mM rifamycin SV. After aspirating the pre-incubation buffer, 0.5 mL of incubation buffer containing substrate was added in the absence or presence of rifamycin SV. The uptake was terminated at a designated time by adding 0.5 mL of ice cold standard HBSS after removal of the incubation buffer. Cells were then washed three times with 0.5 mL of ice cold HBSS. The hepatocytes were lysed with methanol containing the internal standard for LC-MS/MS quantification.

LC-MS/MS Analysis of Probe Substrates. Bosentan was analyzed on an SCIEX Triple Quad 6500 mass spectrometer (SCIEX, Framingham, MA) that is connected to a SLC-30A LC system (Shimadzu, Kyoto, Japan) and HTC PAL autosampler (LEAP Technologies, Carrboro, NC). Samples (10 µL) were injected onto a Kinetex C18 column (2.6 µm, 100Å, 30 × 3 mm, Phenomenex, Torrance, CA) and eluted by a mobile phase with initial conditions of 10% solvent B for 0.2 minute, followed by a linear gradient of 10% solvent B to 100% solvent B over 3.8 minutes (solvent A: 100% water with 0.1% formic acid; solvent B: Acetonitrile/water (90/10, v/v) with 0.1% formic acidv), holding at 100% solvent B for 0.5 minute, and re- equilibration for 1.7 minutes at a flow rate of 0.4 mL/min. The mass transition in positivee ion mode for monitoring bosentan was m/z 552.2→ 202.

Methods for monkey and rat pharmacokinetic and terminal studies

Animals. Male wistar-hannover rats (weighing 230–350 g) studies with surgically implanted vascular cannulas in the jugular vein catheter and/or carotid artery catheter were conducted at Bioduro (Beijing, China). Rats were housed one per cage in an American Animal Association Laboratory Animal Care accredited facility and maintained under standard conditions of temperature (22 °C ± 2°C), relative humidity (50%) and light and dark cycle (12/12 hours). Rats were allowed to acclimate to their environment. Intravenous bolus (i.v.) and intravenous infusion (i.v. inf.) dosed rats had access to water ad libitum. Male cynomolgus monkeys (weighing 8–10 kg) studies were conducted in-house. Monkeys were housed one per cage in an American Animal Association Laboratory Animal Care accredited facility and maintained under standard conditions of temperature (22 °C ± 2°C), relative humidity (50%) and light and dark cycle (12/12 hours). All animal experiments were in accordance with the animal care and use committee of Pfizer Inc.

Protocol for pharmacokinetics and tissue exposure studies in rats. The pharmacokinetic profile of bosentan following i.v. administration was evaluated in wistar-hannover rats. The animals were randomly distributed into five experimental groups (n=2/group). Bosentan was formulated in 12.5% sulfobutylether-beta-cyclodextrin (SBECD) / 50mM Tris, pH 8.0 (v/v). The i.v. bolus treatment groups were dosed with a single dose of 0.1, 0.3, 1, 3, and 10 mg/kg via tail vein. The injection volume was 2 mL/kg. Blood samples were withdrawn from the jugular vein catheter predose, and at the following time points after dosing, 0.033, 0.083, 0.25, 0.50, 1, 2, 4, 7, and 24 hrs. After each blood draw, a volume of sterile normal saline (0.9% sodium chloride, USP containing 100 unit/mL heparin) equivalent to the volume of blood drawn was injected via carotid artery cannula to maintain a constant blood volume (0.25 mL). All blood samples were immediately centrifuged at 3000 rpm for 10 minutes. The resultant plasma was stored at –80°C until bosentan Liquid Chromatography-Mass Spectrometry (LC-MS/MS) analysis.

The tissue distribution profile of bosentan following i.v. infusion administration was evaluated in wistar-hannover rats (n=3). Bosentan was formulated in 12.5% SBECD / 50mM Tris, pH 8.0 (v/v). The i.v. infusion treatment group was dosed at 3.5 m/kg for 4 hours via jugular vein catheter. Blood samples were withdrawn from the carotid artery catheter during infusion at the following time points 0.50, 1, 2, 3, and 4 hrs. After each blood draw, a volume of sterile normal saline (0.9% sodium chloride, USP containing 100 unit/mL heparin) equivalent to the volume of blood drawn was injected via carotid artery cannula to maintain a constant blood volume (0.25 mL). All blood samples were immediately centrifuged at 3000 rpm for 10 minutes. The resultant plasma was stored at –80°C until bosentan LC-MS/MS analysis. Liver, quad, adipose, brain, and kidney tissues were also harvested at the 4 hrs timepoint at the end of the in-life study. Tissues were rinsed with saline and matted dry. Tissues were kept frozen on dry ice or -80°C until ready for LC-MS/MS analysis.

Protocol for pharmacokinetics and tissue exposure studies in monkeys. The pharmacokinetic profile of bosentan following i.v. administration was evaluated in male cynomolgus monkeys in a crossover manner. The same two animals were dosed i.v. bolus of bosentan with a one week wash period in between each dose groups. Bosentan was formulated in 12.5% SBECD / 50mM Tris, pH 8.0 (v/v). The i.v. bolus treatment groups were dosed with a single dose of 0.1, 0.33, 1, 3.33, 10, and 20 mg/kg via saphenous vein or cephalic vein. The injection volume was 2 or 2.8 mL/kg. Blood samples were withdrawn from the femoral vein at the following time points after dosing, 0.083, 0.25, 0.50, 0.75, 1, 2, 4, 7, and 24 hrs. All blood samples were immediately centrifuged at 3000 rpm for 10 minutes. The resultant plasma was stored at –80°C until bosentan LC-MS/MS analysis.

The tissue distribution profile of bosentan following i.v. bolus administration was evaluated in the same two monkeys that were used for pharmacokinetics assessment; male cynomolgus monkeys. Bosentan was formulated in 12.5% SBECD / 50mM Tris, pH 8.0 (v/v). The i.v. bolus was dosed at 10 m/kg, and the study was terminated at 4 hours post dose. The injection volume was 2 mL/kg. Blood sample (4 hour) was immediately centrifuged at 3000 rpm for 10 minutes. The resultant plasma was stored at –80°C until bosentan LC-MS/MS analysis. Liver, quad, adipose, brain, and kidney tissues were harvested at the 4 hrs timepoint at the end of the in-life study. Tissues were rinsed with saline and matted dry. Tissues were kept frozen on dry ice or -80°C until ready for LC-MS/MS analysis.

The pharmacokinetics profile and tissue exposure evaluation of bosentan was performed using Watson v.7.5 (ThermoFischer Scientific, Philadelphia, PA).

Reference

1. NDA-21-290. Clinical pharmacology and biopharmaceutics review. Center for Drug Devaluation and Research, US Food and Drug Administration. 2001.

2. Peters SA. Appendices. Physiologically-Based Pharmacokinetic (PBPK) Modeling and Simulations. John Wiley & Sons, Inc.; 2012. p. 407-21.

3. Yang J, Jamei M, Yeo KR, Tucker GT, Rostami-Hodjegan A. Prediction of intestinal first-pass drug metabolism. Curr Drug Metab. 2007;8(7):676-84.

4. Shah DK, Betts AM. Towards a platform PBPK model to characterize the plasma and tissue disposition of monoclonal antibodies in preclinical species and human. J Pharmacokinet Pharmacodyn. 2012;39(1):67-86. doi:10.1007/s10928-011-9232-2.

5. Bi YA, Scialis RJ, Lazzaro S, Mathialagan S, Kimoto E, Keefer J et al. Reliable Rate Measurements for Active and Passive Hepatic Uptake Using Plated Human Hepatocytes. AAPS J. 2017;19(3):787-96. doi:10.1208/s12248-017-0051-2.